Microstructure and adhesion strength quantification of PVD bi-layered ZnMg-Zn coatings on DP800 steel

Sabooni, S.; Galinmoghaddam, E.; Ahmadi, M.; Westerwaal, R. J.; van de Langkruis, J.; Zoestbergen, E.; De Hosson, J. Th M.; Pei, Y. T.

Published in:
Surface and Coatings Technology

DOI:
10.1016/j.surfcoat.2018.12.064

Surface & Coatings Technology 359 (2019) 227–238

Contents lists available at ScienceDirect

Surface & Coatings Technology

journal homepage: www.elsevier.com/locate/surfcoat

Microstructure and adhesion strength quantification of PVD bi-layered ZnMg-Zn coatings on DP800 steel

S. Sabooni[a,1], E. Galinmoghaddam[a,1], M. Ahmadi[a], R.J. Westerwaal[b], J. van de Langkruis[b], E. Zoestbergen[b], J.Th.M. De Hosson[c], Y.T. Pei[a,*]

[a] Department of Advanced Production Engineering, Engineering and Technology Institute Groningen, Faculty of Science and Engineering, University of Groningen, Nijenborgh 4, 9747 AG, the Netherlands
[b] Tata Steel Nederland Technology B.V., P.O. Box 1000, 1970 CA IJmuiden, the Netherlands
[c] Department of Applied Physics, Zernike Institute for Advanced Materials, Faculty of Science and Engineering, University of Groningen, Nijenborgh 4, 9747 AG Groningen, the Netherlands

ARTICLE INFO

Keywords:
ZnMg-Zn bi-layer coatings
Microstructure
Adhesion strength
Scratch test
Finite element simulation

ABSTRACT

In this study, ZnMg-Zn bi-layered coatings with different Mg contents, a single layer ZnMg coating and a pure zinc coating are deposited on steel substrates by physical vapor deposition (PVD) process. A set of experiments and simulations are performed to study the microstructure, mechanical properties and adhesion behavior of the PVD coatings. It is found that Mg_2Zn_{11} and $MgZn_2$ form in the microstructure of the ZnMg top layer with increasing Mg content. $MgZn_2$ fully covers the microstructure at 14.1 wt% Mg. Scratch tests are carried out to quantify the adhesion strength of the coatings. It is observed that ZnMg single layer coating shows poor adhesion to the steel substrate and the addition of a Zn interlayer is essential for enhancing the adhesion strength. It was found that the measured critical load (L_C) in scratch test is not a suitable criterion to evaluate the adhesion strength of ZnMg-Zn bi-layer coatings with different combination of thickness and/or mechanical properties. Instead, the Benjamin-Weaver model is modified to quantify the adhesion strength at ZnMg/Zn interface by scratch test revealing consistent results with the BMW crash adhesion test (BMW AA-M223) currently used in industry for adhesion qualification.

1. Introduction

In the automotive industry, protection of the car body from corrosion and degradation is critical. This ensures long-term durability of the material, satisfies safety and aesthetic requirements and enables car manufacturers to extend product warranty. Zinc coatings have proven to be the material of choice for protection of steels from corrosion by sacrificial cathodic protection and also by the formation of a superficial barrier coating to shield the steel against corrosive environment [1]. Conventional application of zinc coatings on steel is typically deposited by hot-dip galvanizing (HDG) and electrodeposition [1,2]. It turns out that interfacial compound formation is always a critical issue as far as the adhesion of the coating is concerned. In particular it is shown [3] that the adhesion of hot dip galvanized zinc coatings on dual phase steel can be enhanced by suppressing the formation of Fe-Zn compounds and oxides at the interface between the zinc coating and the steel substrate.

In recent decades, many attempts have been carried out to further improve the corrosion resistance of zinc coatings on steel substrate. Primarily, these efforts led to the advent of zinc alloys containing relatively high amount of aluminum as Galvalume (55 wt% Al) and Galfan (5 wt% Al) [4]. Later, it was discovered that alloying of pure zinc with even small amounts of magnesium considerably increases corrosion resistance of the zinc coating and consequently several Mg-alloyed Zn/Zn-Al coatings were developed [5,6]. Red rust formation of Zn-Mg alloy coated steel was compared to several other Zn binary systems like Zn-Al, Zn-Ti, Zn-Ni and Zn-Cr. Noticeably, It is reported that ZnMg coating exhibited up to 24 times better corrosion performance in salt spray test as compared to electrogalvanized steel while having only half of the applied coating thickness of that of the electrogalvanized sample [7]. Similar salt spray test conducted on ZnMg coated steel at room temperature showed a roughly 5 times better corrosion performance as compared to zinc-plated steel. With increasing test temperature (by 10 °C), the red rust formation time for magnesium-containing coating was 10 times longer than zinc-plated steel [8–10]. Not only for salt

* Corresponding author.
E-mail address: Y.Pei@rug.nl (Y.T. Pei).
[1] Equally contributing to this work.

https://doi.org/10.1016/j.surfcoat.2018.12.064
Received 15 October 2018; Received in revised form 11 December 2018; Accepted 14 December 2018
Available online 15 December 2018
0257-8972/

Table 1
Chemical composition (wt%) of DP800 and black plate steels.

	C	Si	Mn	P	S	Ni	Cr	Cu	Fe
DP800	0.153	0.386	1.487	0.013	0.007	0.018	0.022	0.015	Bal.
Black plate	0.04–0.08	0.03	0.18–0.35	0.02	0.03	0.08	0.08	0.08	Bal.

spray tests, but also during standard automotive cyclic corrosion tests, superior corrosion performance of Mg-alloyed zinc coating was observed [11]. Various theories have been proposed to explain the role of alloying elements in enhancing the corrosion resistance of zinc coatings. It is widely accepted that the presence of alloying elements such as magnesium will promote the formation of simonkolleite ($Zn_5(OH)_8Cl_2{\cdot}H_2O$), a dense corrosion product that in Zn coatings also known as zinc hydroxy carbonate (ZHC), in corrosive environments [12,13].

New challenges arise for the production of ZnMg alloy coatings by conventional processes with the development of next generation steels (NGS) such as advanced and ultrahigh strength steels. Segregation of the alloying elements (mostly Mn, Si and Al) on the surface of NGS during the annealing process, leads to the formation of surface oxides prior to HDG [14]. These surface oxides reduce the wettability and consequently the adhesion of the Zn coating to the steel substrate is reduced. On the other hand, the addition of high Mg content to the zinc bath is not possible. Electroplating is also less effective due to the high energy cost, environmental impact and also the risk of hydrogen embrittlement [15]. Physical vapor deposition (PVD) is a promising alternative method to deposit ZnMg coatings on NGS compared to HDG or electrodeposition. PVD is capable of being performed at much lower substrate temperatures (~250 °C). At such low temperature ranges, detrimental interface reactions and microstructural evolutions and other high-temperature related issues are minimized. Furthermore, production of multilayered coatings with virtually any alloy compositions is feasible. In addition, PVD is conducted in a closed vacuum chamber and does not involve using hazardous chemicals (as in electroplating), it fulfills strict environmental regulations [16].

Most of the studies about ZnMg coatings are mainly focused on the corrosion resistance properties and just a few researches have been conducted to study the adhesion performance of ZnMg coatings to steel substrate. Lap shear and 180° bending tests were performed to study the effect of Mg content on the adhesion behavior of single layer PVD ZnMg coatings [17]. Coatings containing < 5 wt% Mg exhibited good adhesion with ductile fracture mode while for the coatings with higher Mg contents, poor adhesion with brittle fracture was observed. A semi-quantitative evaluation of the adhesion of ZnMg coating was conducted by a combination of punch stretching and potentio-dynamic polarization tests [18]. It was found that the variation of corrosion potential after deformation is closely related to the coating adhesion. The results showed that the adhesion of ZnMg coatings to steel decreases with increasing the Mg content. The formation of brittle intermetallic compounds such as Mg_2Zn_{11} and $MgZn_2$ is reported to be a possible reason for the adhesion degradation in ZnMg single layer coatings. The loss of adhesion causes coating delamination during subsequent production processes such as punching, bending and press forming. Lee et al. [19] studied the effect of Al interlayer insertion on the adhesion properties of ZnMg thin films and reported strong adhesion between Al interlayer and ZnMg top layer due to the pure metallic bonding.

Several strategies can be used to improve the adhesion of PVD ZnMg coating to steel substrate such as plasma pre-cleaning in vacuum, addition of a ductile interlayer and also chemical composition modification. Although a few examinations [17,19] have been done previously to understand the adhesion behavior of ZnMg coatings, there is still lack of knowledge about the quantitative analysis of the adhesion strength and also the exact role of chemical composition on the adhesive properties. To fill this gap, a set of experiments and simulations were performed in the present work to study the microstructure, mechanical properties and adhesion behavior of ZnMg PVD coatings as a function of Mg content. A modified Benjamin-Weaver model has been used to calculate the adhesion strength of bi-layer coatings using scratch tests.

2. Materials and methods

Two different types of steels (DP 800 dual phase steel and black plate steel) sheets 0.2 mm thick were used as substrates for this investigation. The chemical composition of each substrate is shown in Table 1.

Pure zinc and ZnMg layers were produced by a thermal evaporation PVD machine. The vacuum chamber of the machine was equipped with two crucibles containing pure zinc and ZnMg. Before coating deposition, the surface of the steel strip is pretreated to remove surface oxides and preheat the strip. The evaporator uses an induction coil system to thermally evaporate the pure or alloyed melt. The metal vapor passes through a vapor distribution box (VDB) and deposits on the surface of the running steel strip. Pure zinc, single layer ZnMg and bi-layer ZnMg-Zn coatings were produced for study. All of the ZnMg-Zn bi-layered coatings were deposited on DP800 substrate and the black plate steel was just used to deposit pure zinc and single layer ZnMg for comparison. The ZnMg top layers are named as ZnMgx with x indicating the Mg content in weight percent.

Grazing angle X-ray diffraction (GAXRD) was used to identify phase constituents of the ZnMg coatings with different Mg contents. The incidence angle was selected as 2° for all the XRD experiments to discard the effect of Zn interlayer. Phase fraction analysis was also performed for quantification. The surface morphology and coatings' microstructure were studied by scanning electron microscopy (SEM-Philips XL30 ESEM). In-situ SEM tensile tests (Kammrath & Weiss 5000 N Tensile and Compression Module) were performed to evaluate mechanical properties of the ZnMg coatings. Fig. 1 shows the configuration of the in-situ stage and the tensile specimen.

Nanoindentation tests were performed using MTS Nanoindenter XP equipped with Berkovich diamond indenter in both load control and depth control modes. A minimum of 30 indentations were carried out for every test to measure the hardness and the elastic modulus.

CSM Revetest scratch tester was used to evaluate the adhesion strength of different ZnMg coatings. In this test, a diamond stylus (Rockwell C, 200 μm in radius) is drawn along the coating with progressively increasing normal load to generate a distinct failure (continuous delamination) at a critical load (L_C). The maximum load of 20 N was used for all the ZnMg coatings, with 20 N/min loading rate and 10 mm scratch length. For the pure zinc coating, the maximum load and the loading rate were 50 N and 50 N/min, respectively. A minimum of 5 scratch tracks were made for each coating and the average value of L_C was reported. An ion beam cryo cross-section polisher (JEOL IB-19520CCP) was used to scrutinize failures in the scratch track. The sample during ion polishing was kept at −140 °C to avoid any possible defect induced by ion polishing on the coatings and/or interfaces. BMW crash adhesion tests (BMW AA-M223) were also performed for qualitative evaluation of the adhesion of the coatings. This test is a bending-based standard method currently used in industry to qualify the adhesion behavior of galvanized coatings. To pass the test, the adhesively bonded joint should fail in the adhesive, not in the coating/substrate interface. More information about this test can be found elsewhere [20].

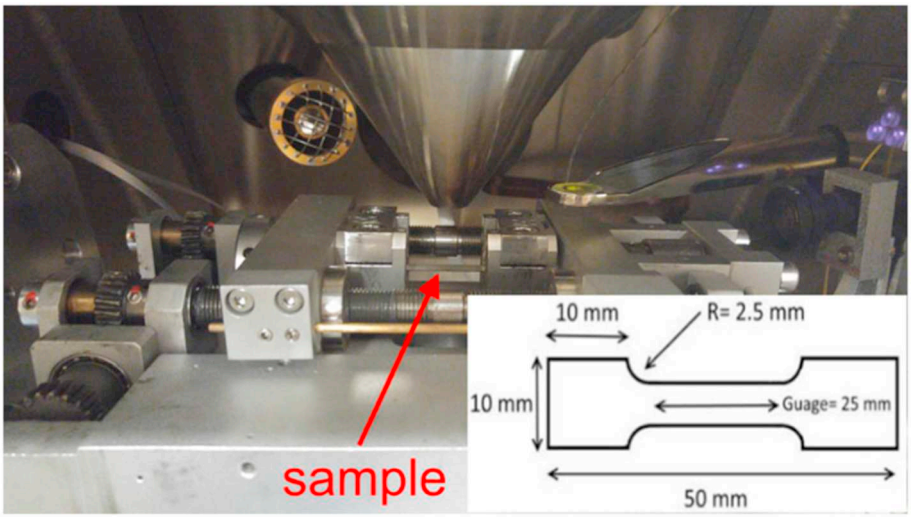

Fig. 1. Configuration of in-situ SEM tensile test.

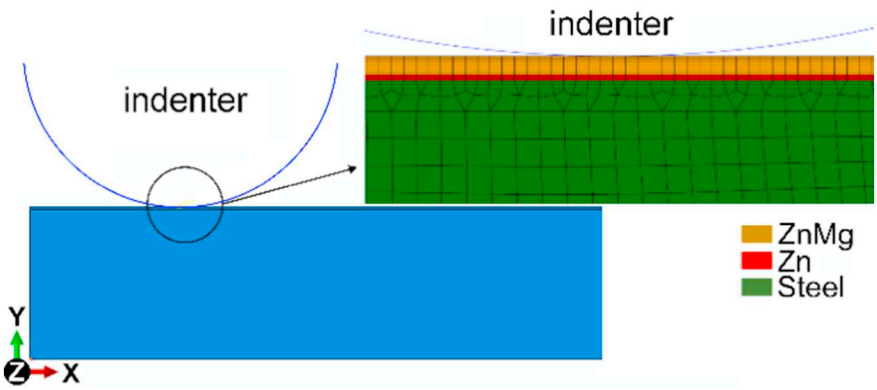

Fig. 2. Geometry of the FEA of the scratch test on bi-layer ZnMg-Zn coated sample.

Finite Element Analysis (FEA) was used to simulate the behavior of coated samples during scratch test. Two distinct simulations were performed for single layer ZnMg coated and bi-layer ZnMg-Zn coated steel substrates. Fig. 2 illustrates the geometries and sections of the model. A dynamic explicit two dimensional (2D) plane stress simulation was considered. The indenter was selected as a rigid body with 200 μm radius while the substrate and the coatings were defined as deformable homogenous solids with individual allocated properties. The mechanical properties of the ZnMg coating were obtained by nanoindentation and implemented into the model. For the bi-layer coating, the thicknesses of zinc interlayer and ZnMg top layer were selected as 1 μm and 3 μm, respectively. The thickness of the ZnMg coating was kept constant in the case of the single layer coating. The sample was fixed against all rotations and displacements. The same scratch parameters (maximum load, loading rate and scratch distance) were defined in the simulation according to the experiments. Mesh refinement (2 × 0.4 μm) was utilized in the coating regions for a better resolution. To model the failure mechanism of the coatings, ductile shear damage behavior was assumed. In order to avoid severe mesh distortion, Arbitrary Lagrangian-Eulerian (ALE) mesh control was employed in accordance with the simulation steps.

3. Results and discussion

3.1. Microstructure and phase analysis

Fig. 3a shows the XRD patterns of PVD ZnMg layers with different Mg concentrations in the range of 1.5–14.1 wt%. Quantification of phase contents is shown in Fig. 3b. The ZnMg layers are mostly composed of pure zinc when the Mg concentration is low (1.5 wt%). The fraction of zinc phase decreases with increasing the Mg content and simultaneously the Mg_2Zn_{11} fraction increases. Further increase in the Mg content (≥5.8 wt%) results in a full content of intermetallic compounds (mixture of Mg_2Zn_{11} and $MgZn_2$). The phase fraction of $MgZn_2$ increases with Mg content and becomes the only observable phase at 14.1 wt% Mg. Different microstructures were reported in the literature for the ZnMg coatings with high Mg content. La et al. [21] reported amorphous phase formation during magnetron sputtering of Zn-15.8 wt % Mg. Extended solid solubility of Mg atoms during magnetron sputtering and the resulting local lattice distortion are reported as the main reasons for the structural change from crystalline to amorphous for high Mg content coatings [21]. The same behavior is also reported by Lee et al. [19] for the formation of amorphous phase in the PVD coated Zn-14 wt% Mg. On the other hand, a crystalline mixture of Mg_2Zn_{11} and $MgZn_2$ was observed for the electromagnetic levitated PVD Zn-15 wt% Mg coating [17].

Since amorphous and/or crystalline microstructures are reported for highly alloyed ZnMg coatings produced by different methods, “Miedema thermodynamic model” [22,23] and “Egami and Waseda model” [24] were used to predict the stability of amorphous phase in the Zn-Mg binary alloy system. According to Miedema semi-empirical model, the formation enthalpy of an amorphous phase consists of two terms:

$$\Delta H_{amorphous} = \Delta H_{chemical} + \{3.5 \times 10^{-3} (T_m^{average})\} \quad (1)$$

$\Delta H_{chemical}$ represents the chemical contribution due to the electron

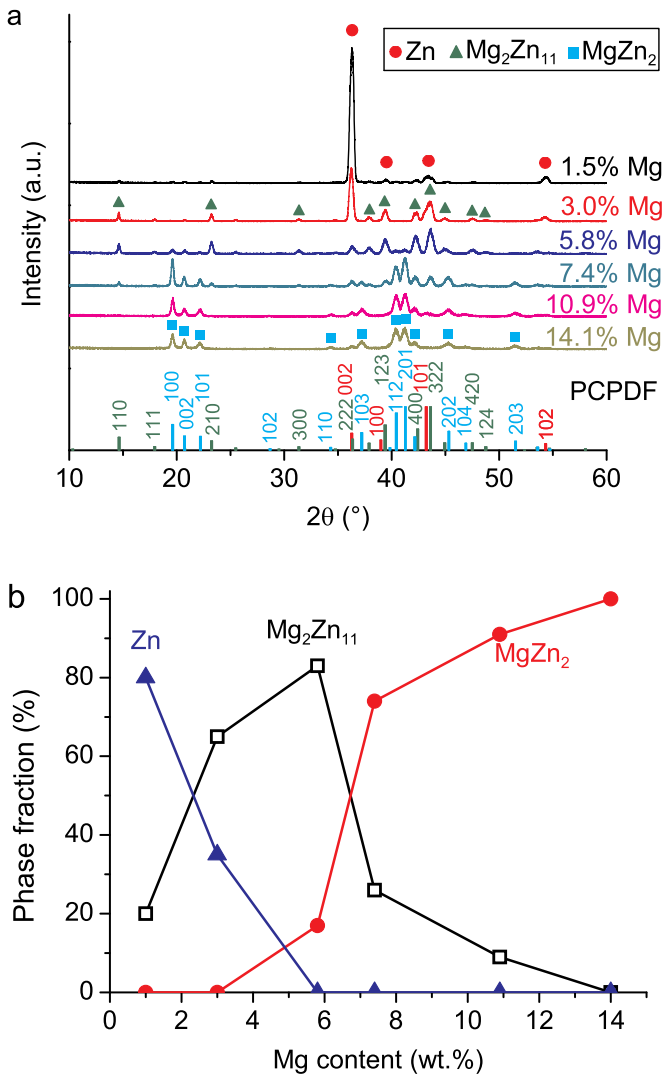

Fig. 3. (a) XRD patterns and (b) phase content of PVD ZnMg-Zn bi-layer coatings.

redistribution that occurs when an amorphous alloy is formed. This term can be calculated as follows:

$$\Delta H_{chemical} = X_A X_B \left(f_A^B \Delta H_{int}^{B\ in\ A} + f_B^A \Delta H_{int}^{A\ in\ B}\right) \quad (2)$$

where f_B^A and f_A^B show the degree to which A atoms are surrounded by B atoms and vice versa, and are calculated by the following equations:

$$f_B^A = X_B^S\left(1 + \gamma (X_A^S X_B^S)^2\right) \quad (3)$$

$$X_A^S = \frac{X_A V_A^{2/3}}{X_A V_A^{2/3} + X_B V_B^{2/3}} \quad (4)$$

$$X_B^S = \frac{X_B V_B^{2/3}}{X_A V_A^{2/3} + X_B V_B^{2/3}} \quad (5)$$

where X and V represent molar fraction and molar volume of elements in the chemical composition. γ is an empirical parameter which is considered as 5 for an amorphous phase [25].

$\Delta H_{int}^{A\ in\ B}$ and $\Delta H_{int}^{B\ in\ A}$ are the interfacial enthalpy during mixing of A atoms in B and B atoms in A, respectively, and can be calculated as

$$\Delta H_{int}^{A\ in\ B} = \frac{2P V_A^{2/3}}{\left(n_{ws}^{-\frac{1}{3}}\right)_A + \left(n_{ws}^{-1/3}\right)_B}\left\{-(\Delta\varphi^*)^2 + \frac{Q}{P}\left(\Delta n_{ws}^{\frac{1}{3}}\right)^2\right\} \quad (6)$$

Table 2
Parameters required for Miedema thermodynamic calculations in Zn-Mg binary system [25–27].

Element	T_m (K)	$n_{ws}^{1/3}$ (d.u.)$^{1/3}$	φ^* (eV)	$V^{2/3}$ (cm^2/mol)
Zn	692	1.32	4.1	4.38
Mg	923	1.17	3.45	5.80

$$\Delta H_{int}^{B\ in\ A} = \frac{2P V_B^{2/3}}{\left(n_{ws}^{-\frac{1}{3}}\right)_A + \left(n_{ws}^{-1/3}\right)_B}\left\{-(\Delta\varphi^*)^2 + \frac{Q}{P}\left(\Delta n_{ws}^{\frac{1}{3}}\right)^2\right\} \quad (7)$$

where φ^* is the work function of elements and n_{ws} is their electron density. P and Q are constants depending on the type of elements ($P = 10.6$, $Q/P = 9.4$ in units of eV^2/(d.u.)$^{2/3}$) [25].

$T_m^{average}$ is the average melting temperature of the binary compound and is estimated as follows [26]:

$$T_m^{average} = (X_{Zn} \times T_m^{Zn} + X_{Mg} \times T_m^{Mg}) \quad (8)$$

where T_m^{Zn} and T_m^{Mg} represent the melting temperatures of pure zinc and magnesium, respectively. The required parameters for thermodynamic calculations are presented in Table 2.

A critical note here concerns the description of the interfacial enthalpy in terms of the differences in work functions $\Delta\varphi^*$ and electron density $\Delta n_{ws}^{\frac{1}{3}}$ (see Eqs. (6) and (7)). In essence it is assumed that the enthalpy consists of two contributions: a negative one, reflecting flow of charge between A and B which generates a dipolar layer and a positive one because the equilibrium charge densities in A and B become out of equilibrium (discontinuity will raise energy). So, basically it is an ionic rigid band model description of a metallic system, which unfortunately provides the wrong picture. We argue that the heat of formation in metals arises from common band formation (attractive) and a change in bond length (repulsive). As a consequence it is cannot be described by any ionic band model. However, it is fair to say that the Miedema model can still be useful (not because of the correct description of the origin of bonding in metals though). The strength of the approach rests in its compatibility with known experimental data and its ease of applicability to a multitude of problems in alloy cohesion. Indeed, far better physical models can elucidate the origin of bonding in metals and (crystalline and amorphous) alloys but they do not replace phenomenological schemes. Therefore the following should be considered as a "phenomenological" description, i.e. useful for its application to describe interface strength between heterophases, but not providing the correct physical description of the actual cause of bond strength in metallic systems.

Enthalpy change during the formation of the amorphous phase in Zn-Mg binary system is shown in Fig. 4. As seen, there is no tendency for the formation of amorphous phase when the molar fraction of zinc is very high or very low. However, the enthalpy change for the formation of amorphous phase is negative between 29–82 at.% Zn (i.e. 7.5–49 wt % Mg), indicating that the formation of amorphous phase is feasible.

Egami and Waseda model [24] was also used to predict the possible range for the formation of amorphous phase in Zn-Mg binary alloy system and to compare with the Miedema thermodynamic model. According to this model, the minimum concentration of solute atoms for the formation of amorphous phase can be determined by

$$C_{min} \times |volume\ mismatch| \cong 0.1 \quad (9)$$

where C_{min} is the minimum concentration of the solute atoms required for the formation of amorphous phase. Volume mismatch can also be calculated by

$$\text{Volume mismatch} = \left(\frac{R_B}{R_A}\right)^3 - 1 \quad (10)$$

where R_A and R_B are the radius of the matrix and solute atoms, respectively. In order to obtain the glass forming range for ZnMg

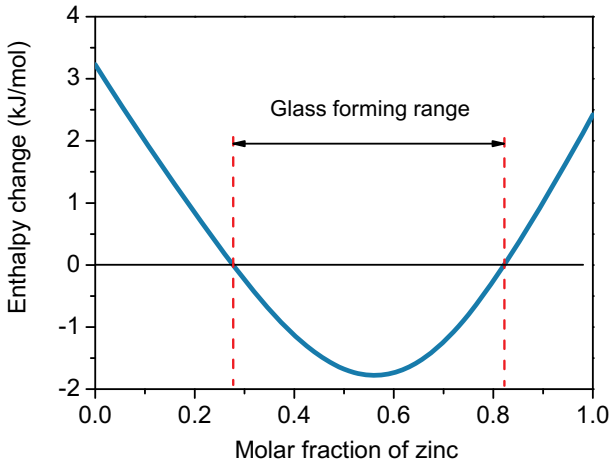

Fig. 4. Enthalpy change during the formation of amorphous phase in Zn-Mg binary system.

compounds, it is necessary to consider both Zn-rich and Mg-rich regions. It is interesting to note that the glass forming range in Zn-Mg binary system calculated based on the Egami model is exactly the same as predicted by Miedema thermodynamic model (7.5–49 wt% Mg).

Although the composition range for the formation of amorphous phase is predicted as 7.5–49 wt% Mg, no amorphous phase is detected in the XRD pattern of the thermally evaporated ZnMg coatings of that composition range in the present investigation. However, transition of amorphous to crystalline microstructure has been previously reported for the magnetron sputtered ZnMg coatings containing ~12.6 wt% Mg, where the coatings sputtered below 50 °C exhibited a featureless amorphous structure while a crystalline microstructure was formed by increasing the deposition temperature to 100 °C [21]. The adhesion strength of amorphous ZnMg to the mild steel substrate was unsatisfactory, but improved after increasing of the deposition temperature meaning that the adhesion strength of the coating improves by crystallization of the amorphous structure [21]. Therefore, the presence of crystalline Mg_2Zn_{11} and $MgZn_2$ intermetallics in the microstructure of the produced coatings is favorable for sound adhesion. Possible reasons for crystalline microstructure in the thermally evaporated ZnMg PVD coatings of the present work might arise from the effect of vacuum plasma cleaning in the PVD process, radiation heating induced by the hot VDB and also the released heat during de-sublimation of ZnMg vapor. In this study, the temperature of the steel strip by PVD process reached ~260 °C, seems to be adequate to crystallize the amorphous microstructure.

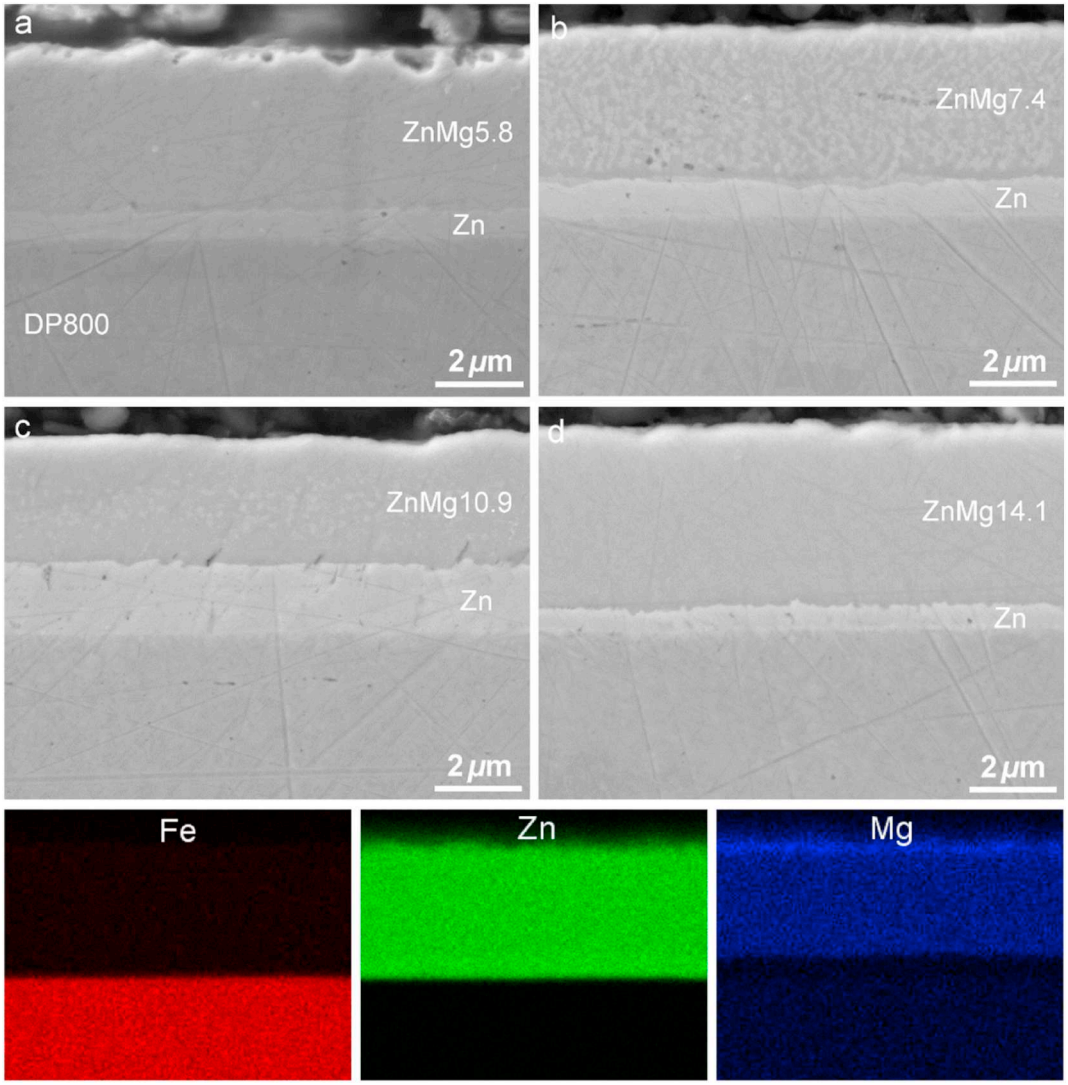

Fig. 5. Cross sectional SEM micrograph of ZnMg-Zn bi-layer coatings with different Mg contents in the top ZnMg layer: (a) 5.8 wt% Mg, (b) 7.4 wt% Mg, (c) 10.9 wt% Mg and (d) 14.1 wt% Mg, along with the elemental mapping of ZnMg5.8-Zn bi-layered coating (bottom row).

Table 3
Adhesion strength of pure Zn and ZnMg-Zn coatings containing different Mg contents using scratch test.

Coating	Zn thickness (μm)	ZnMg thickness (μm)	Critical load L_C (N)	Residual depth at L_C (μm)	Weight factor ω	Adhesion strength (MPa)	BMW adhesion test
Pure zinc	4.9	0	38.5 ± 1.5	–	–	171	Pass
ZnMg5.8-Zn	0.7	3.9	18.1 ± 0.6	4.3	0.16	129	Pass
ZnMg7.4-Zn	0.9	3.7	13.2 ± 0.7	3.3	0.27	103	Pass
ZnMg10.9-Zn	1.6	3.1	9.3 ± 0.6	2.0	0.80	54	Not pass
ZnMg14.1-Zn	0.6	4.4	8 ± 0.6	1.9	0.31	78	Pass

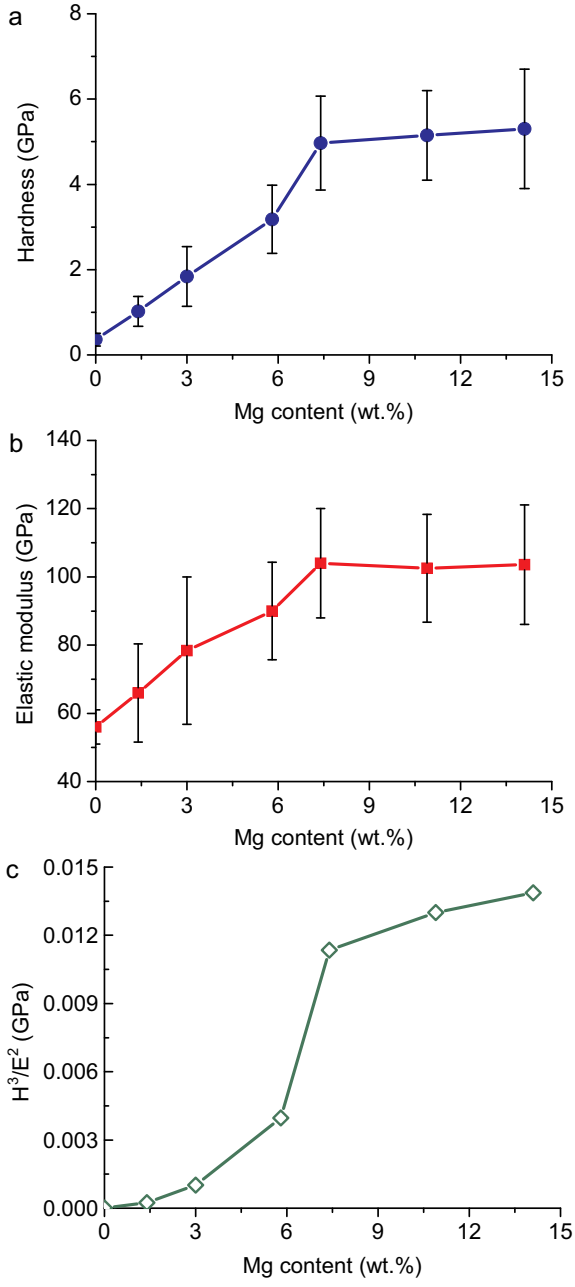

Fig. 6. (a) Hardness, (b) elastic modulus and (c) H^3/E^2 ratio of the ZnMg-Zn bi-layer coatings of different Mg contents deposited on DP800 steel.

Fig. 5 shows the cross sectional SEM micrographs of the ZnMg-Zn bi-layer coatings with different Mg concentrations. The thicknesses of the zinc interlayer and the ZnMg top layer for each coating are presented in Table 3. The ZnMg5.8 top layer consists mainly of the Mg_2Zn_{11} phase. The elemental mapping of ZnMg5.8-Zn bi-layered coating is also presented in Fig. 5. The two phase microstructure

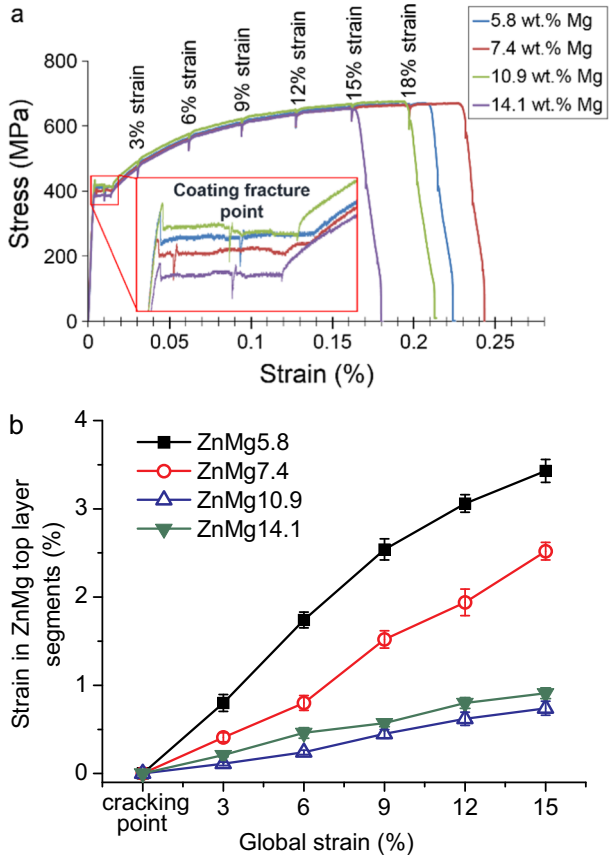

Fig. 7. (a) In-situ tensile stress-strain curve of different ZnMg-Zn bi-layer coatings coated DP800 steel, (b) ZnMg top layer strain after cracking point versus global strain calculated by images processing.

consisting of Mg_2Zn_{11} and $MgZn_2$ intermetallic compounds is clearly visible in the ZnMg7.4 top layer. The concentration of Mg_2Zn_{11} phase decreases with further increase in Mg content, and the ZnMg14.1 top layer is fully composed of $MgZn_2$, which is consistent with the XRD result.

3.2. Mechanical properties

Nanoindentation tests were carried out on the surface of the coatings to determine their mechanical properties. The obtained hardness and elastic modulus from depth sensing indentation are presented in Fig. 6. It should be noted that the hardness and the elastic modulus of pure zinc PVD coating are 0.36 GPa and 56 GPa, respectively. The hardness and the elastic modulus increase with increasing the Mg content up to 7.4 wt% Mg due to the formation of the intermetallic phases (Fig. 6a–b). The hardness and the elastic modulus of ZnMg7.4-Zn coating are 5 GPa and 103 GPa, respectively. With further increase of the Mg content to 14.1 wt%, the hardness and the elastic modulus of the ZnMg coatings remain almost constant since these ZnMg coatings of beyond 7.4 wt% Mg consist of almost fully $MgZn_2$. A similar hardness

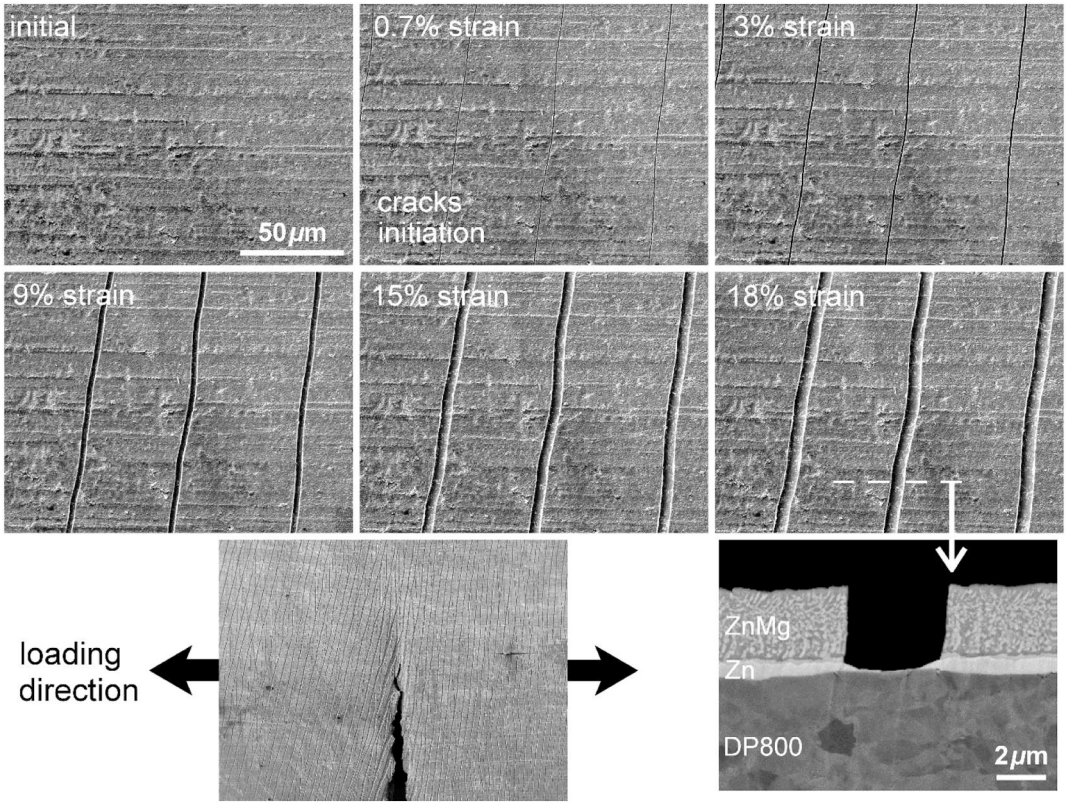

Fig. 8. SEM micrographs of the same view area during in-situ tensile test of ZnMg7.4-Zn bi-layer coated DP800 steel at different global strains, and cross sectional view of a crack in the coating after unloading.

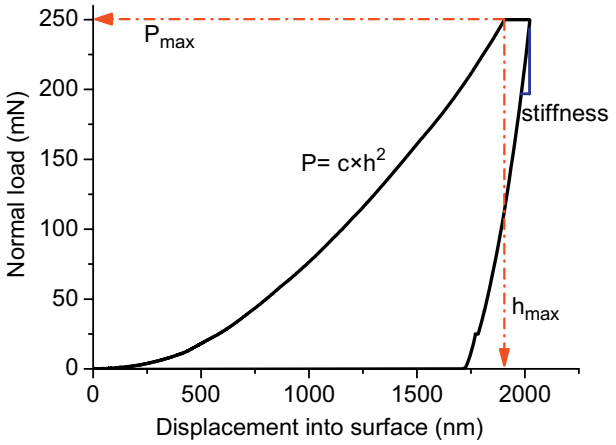

Fig. 9. Nanoindentation load-displacement curve of ZnMg6.8-Zn bi-layer coating (ZnMg layer 7 μm thick) used to calculate σ_y and n for FEA simulation.

value (5.08 ± 0.32 GPa) was previously reported for $MgZn_2$ [28].

The H^3/E^2 ratio can be used as an indication of coating resistance to plastic deformation [29,30]. As seen in Fig. 6c, the value of H^3/E^2 ratio is very small when Mg content is < 3 wt% (Zn is the main constituent phase of the coating). The ratio considerably increases and reaches 0.011 at 7.4 wt% Mg to 0.014 GPa at 14.1 wt% Mg. Clearly, the formation of the intermetallic compounds reduces the ability of the coatings to plastically deform. It is noteworthy that the value of H^3/E^2 ratio for ZnMg coatings is still much lower than the well-known hard coatings such as TiN which has a H^3/E^2 ratio of 0.07–0.49 [30,31].

In-situ SEM tensile tests were performed on PVD ZnMg-Zn bi-layer coated DP800 steel samples to evaluate the tensile behavior of different ZnMg coating alloys (see Fig. 7a). All coatings start to crack within the Lüders band region of the DP800 substrate (< 1.3% of global strain), dividing the coatings into segments about 40 μm wide nearly perpendicular to the loading direction. Cracks opening between the segments gets wider and wider with increasing the global strain. It was observed that each ZnMg segment continues to stretch with further increase in the global strain, indicating that the ZnMg top layer is still under strain after initial partitioning (see Fig. 7b). For instance, at 15% of global strain, 3.4% and 2.6% increase in the strain of ZnMg top layer is observed compared to the cracking point of ZnMg5.8 and ZnMg7.4 coatings, respectively. Those values are higher than the required strain for initial cracking of the coatings (< 1.3% of global strain). However, no further partitioning occurs in the segments until the fracture failure of the steel substrate (Fig. 8). Therefore, it can be concluded that the formation of Lüders band during the tensile test can locally increase the strain, leading to the premature cracking of ZnMg coatings. As can be seen, Zn interlayer is mostly attached on the steel substrate after tensile test and failure occurs at the ZnMg/Zn interface, indicating that the interfacial adhesion between Zn interlayer and steel substrate is always higher than that of the ZnMg/Zn interface. In particular, large shear deformation occurs within the Zn interlayer that has partially been pulled out from/underneath the edges of segments of the top ZnMg coatings.

Nanoindentation was also used to estimate the yield strength (σ_y) and work hardening exponent (n) of ZnMg layer using the reverse analysis algorithm put forward by Dao et.al [32]. This algorithm uses the maximum load (P_{max}), the maximum penetration depth (h_{max}), the curvature of the loading part (c) and the stiffness at the onset of unloading and extracts the σ_y and n (see Fig. 9). Since, the average roughness of the studied ZnMg coatings is around 0.1 μm, a seven micron thick ZnMg coating was selected for the estimation of σ_y and n. The maximum load was set to 250 mN to achieve a penetration depth of ~1.8 μm, to compensate the effect of surface roughness on the load-displacement curve. The calculated σ_y and n for the coating Zn-6.8 Mg is

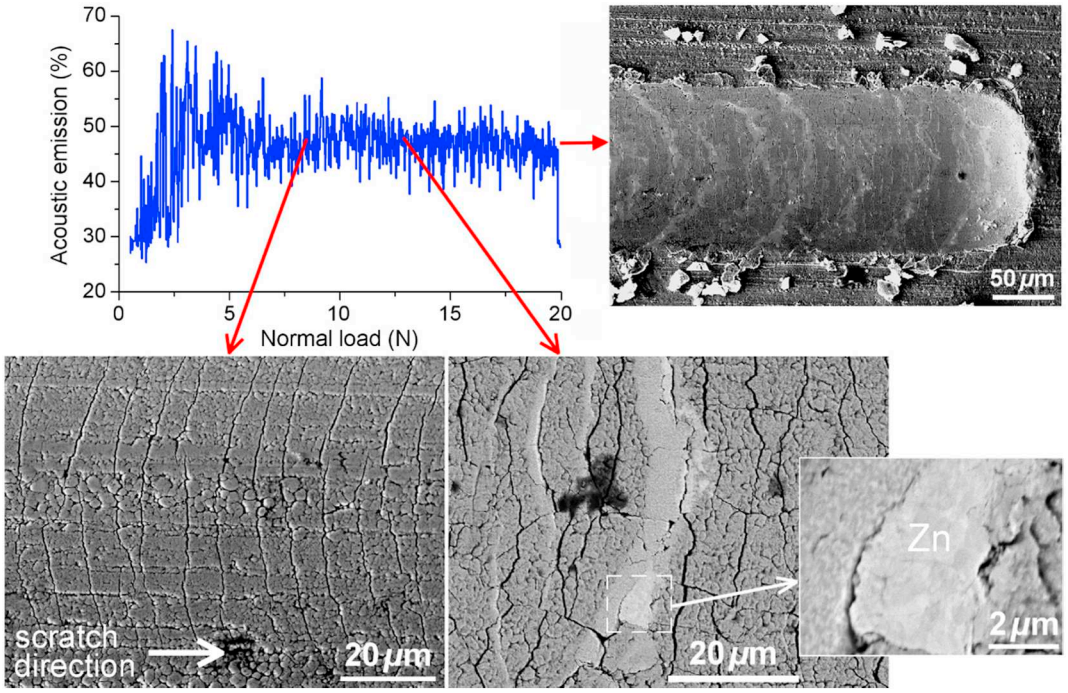

Fig. 10. Acoustic emission versus normal load recorded in scratching ZnMg7.4-Zn bi-layer coating with corresponding SEM micrographs showing the scratched surface at different normal loads.

730 ± 60 MPa and 0.177 ± 0.012, respectively. These values were used in the FEA simulation to investigate the effect of zinc interlayer on the adhesion of the ZnMg coating.

3.3. Adhesion strength

Scratch tests were used to evaluate the adhesion strength of different ZnMg coatings. Fig. 10 shows the acoustic emission curve versus normal load for the ZnMg7.4-Zn bi-layer coating on DP800 substrate and the corresponding SEM micrographs at different normal loads. Tensile cracks are clearly visible at 8 N. Ion beam polishing was used to study the cross section of the observed cracks, shown in Fig. 11. The cracks are propagated through the thickness of the top layer and blunted at the ZnMg/Zn interface. Therefore, it can be concluded that the tensile cracks are only through thickness and are not responsible for the delamination of the top layer. Buckling which is a common failure mode in scratch test is clearly observed at higher normal loads. Ahead of each buckled area, delamination of the top ZnMg layer occurs where the first trace of pure zinc (as interlayer) was observed at around 13 N, which is defined as the critical load L_C. This delamination-buckling behavior continues to higher normal loads up to 20 N.

The critical loads of the pure zinc coating deposited on black plate steel substrate and the ZnMg-Zn bi-layer coatings deposited on DP800 steel substrate, obtained by the scratch test, are presented in Table 3. The L_C for pure zinc coating is 38.5 N, which is much higher than that of the ZnMg-Zn bi-layered coatings. The critical load decreases with increasing Mg content and drops to 8 N for the coating ZnMg14.1-Zn, which has the highest Mg content. BMW crash adhesion test results are also included in Table 3. The coating ZnMg10.9-Zn did not pass the BMW adhesion test. However, its critical load is still higher than that of the coating ZnMg14.1-Zn. It can be concluded that L_C alone is not an appropriate criterion to compare the adhesion of bi-layered ZnMg-Zn coatings of different thickness and/or mechanical properties combinations. It is reported that the critical load depends on many parameters which can be classified as extrinsic (loading rate, scratching speed, radius of the indenter tip) and intrinsic parameters (mechanical properties of the substrate and/or coating, roughness and also friction). For

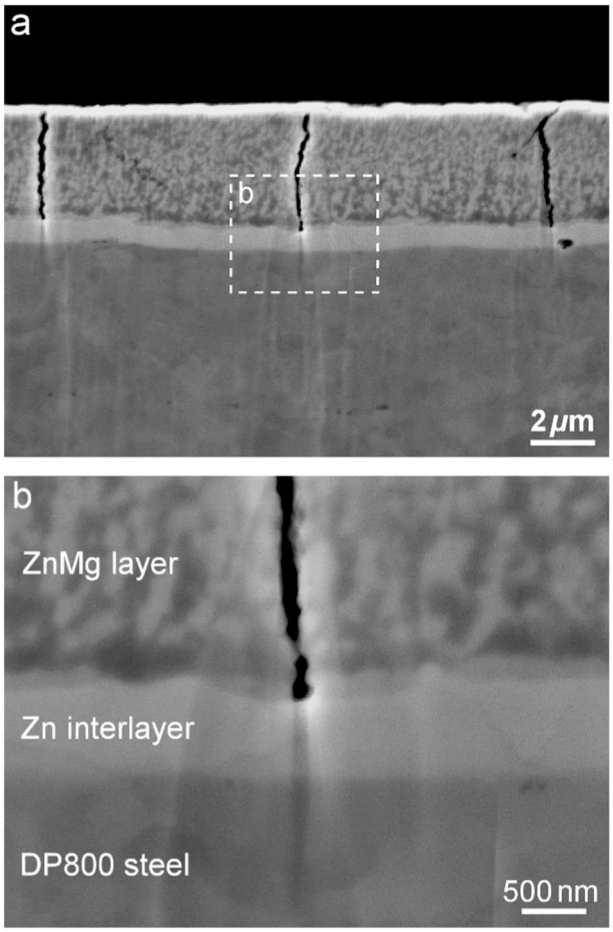

Fig. 11. Cross sectional SEM micrographs of the periodic tensile cracks observed in Fig. 10: (a) overview and (b) close-up showing the blunted tip of a crack.

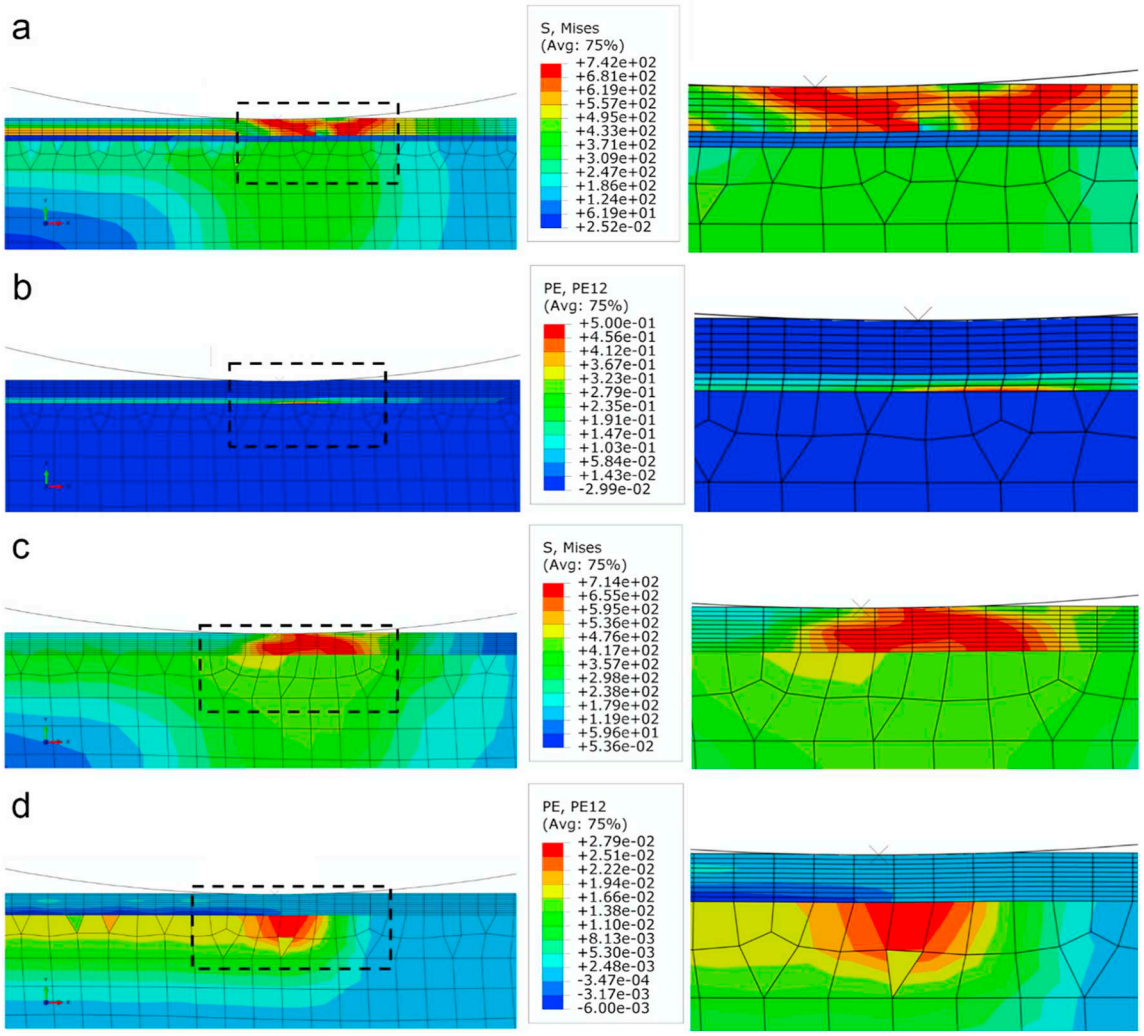

Fig. 12. Finite element simulation of the scratch test prior to coating failure: (a) von Mises stress and (b) shear strain distribution of ZnMg6.8-Zn bi-layer coating on DP800 steel; (c) von Mises stress and (d) shear strain distribution of ZnMg6.8 single layer coating coated DP800 steel. Left column: overview; Right column: close view of the indicated region with a dashed box.

example, the L_C increases with increasing coating thickness or increasing hardness of the substrate [33,34]. Therefore, it is necessary to keep such coating parameters constant or take their effects into account for comparing different samples. Benjamin-Weaver model [35–37] is used to estimate the adhesion strength of ZnMg to the Zn interlayer according to the following equation

$$F = \frac{kaH}{\sqrt{R^2 - a^2}} \tag{11}$$

where F is the adhesion strength (MPa), K is a constant (0.2), R is the radius of the scratch tip, H is the hardness of the substrate and a the radius of the contact circle which is determined as

$$a = \left(\frac{L_c}{\pi H}\right)^{0.5} \tag{12}$$

Benjamin-Weaver model is only valid for coatings having the hardness lower than 5 GPa, which is the case of ZnMg coatings [37]. As concluded before, the addition of pure Zn interlayer is necessary to obtain good adhesion between ZnMg top layer and steel substrate. In the case of the bi-layered coatings, the role of the hardness of both the Zn interlayer and the steel should be considered in Eqs. (11) and (12) as "H". In order to take them into account, a weight factor was proposed as in Eq. (13) and used to determine the composite hardness according to Eq. (14). Definition of the composite hardness is based on the physical understanding that when the ratio of the thickness of the zinc interlayer to the residual scratch depth at the critical load is large, the role of zinc interlayer in the composite hardness would be higher and vice versa.

$$\omega = \frac{\text{Thickness of zinc interlayer}}{\text{Residual depth at } L_C} \tag{13}$$

$$H_{composite} = \omega H_{Zn} + (1 - \omega) H_{steel} \tag{14}$$

Table 3 shows the adhesion strength of the pure zinc and ZnMg coatings with different Mg concentrations determined by the scratch test based on the modified Benjamin-Weaver model. Other properties of the coatings such as the Zn layer thickness, ZnMg layer thickness, residual scratch depth at L_C, weight factor and the BMW crash adhesion test results are also summarized in the table. As can be seen, pure zinc has the highest adhesion strength (171 MPa) among the coatings, comparable with the adhesion strength of hot dip Zn coating on IF steel and TRIP steel which has been previously reported as 180 MPa and 160 MPa, respectively [38,39]. The adhesion strength between ZnMg top layer and Zn interlayer decreases with increasing the Mg content and drops to 54 MPa at 10.9 wt% (coating ZnMg10.9 that has a thick Zn interlayer). In particular, although containing higher Mg content, the coating ZnMg14.1 exhibits higher adhesion strength than the coating ZnMg10.9, partially attributed to the effect of a thicker Zn interlayer employed in ZnMg10.9. It is worthy to note that the results of the

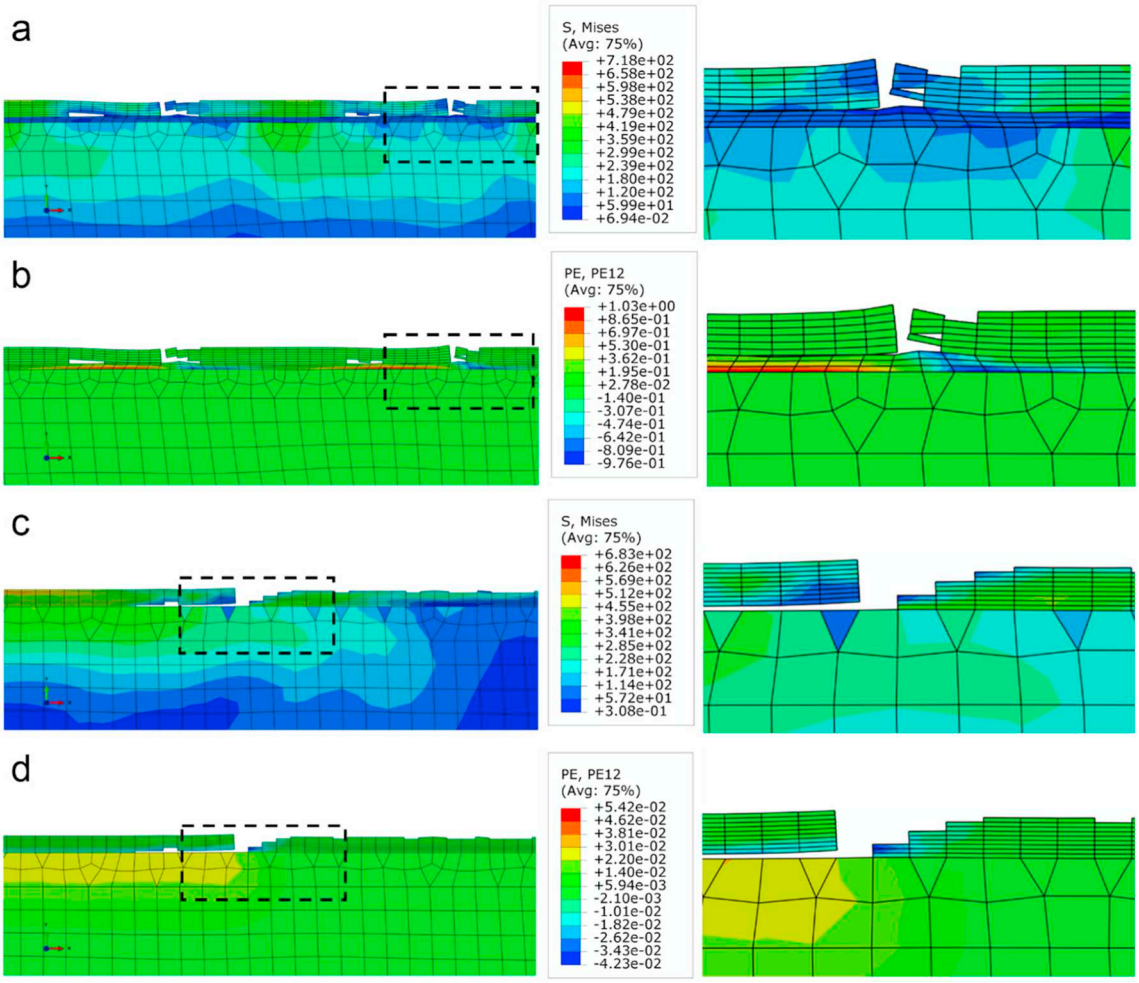

Fig. 13. Finite element simulation of coating failure in scratch test: (a) von Mises stress and (b) shear strain distribution of ZnMg6.8-Zn bi-layer coating on DP800 steel; (c) von Mises stress and (d) shear strain distribution of ZnMg6.8 single layer coating coated DP800 steel. Left column: overview; Right column: close view of the indicated region with a dashed box.

adhesion strength estimated according to the modified model are consistent with the BMW adhesion test where, according to the test, the coating ZnMg10.9 is not qualified. In this perspective it is interesting to note that previous studies on the corrosion behavior of ZnMg coatings showed that the best corrosion performance of the ZnMg coatings was achieved for Mg concentrations in the range of 4–8 wt% which can be 10 times better than pure zinc [40]. When compared to the quantified adhesion strength, the combined highest performance can be achieved in the two coatings with Mg content of 5.8–7.4 wt%, which is in the same range.

Finite element simulations of the scratch test were carried out to further study the failure behavior of the single layer ZnMg and bi-layer ZnMg-Zn coatings. Stress and strain distributions within the sample before the onset of the failure for both single and bi-layer coatings are shown in Fig. 12. As can be noticed in Fig. 12a and c, most of the stress concentration is observed in the ZnMg layer underneath the indenter tip in both the cases. For the bi-layer case (Fig. 12a), there is a remarkable stress concentration between zinc interlayer and the ZnMg top layer resulting in initiation of the damage at the ZnMg/Zn interface. According to Fig. 12b and d, the shear strain distribution in the coatings are also found different for the two simulations. During scratching of the bi-layer coating, most of the shear strain is accommodated in the zinc interlayer, while it mostly spreads to the steel substrate in the single layer case. This observation indicates the effective role of ductile Zn interlayer to withstand the shear strain and plastic deformation during the scratch test which results in maintaining a good adhesion.

The results of the simulation in the initial failure region during the scratch test are given in Fig. 13. These results predict the formation of periodic failure (delamination) in the ZnMg layer during scratching on the bi-layer coating sample (see Fig. 13a and b). The delamination occurs at the ZnMg/Zn interface, whereas no failure is observed at the Zn/steel interface. The mechanism of the periodic failure of the ZnMg top layer can be explained by the simulation result depicted in Fig. 13b. Due to the severe plastic deformation imposed to the coating, when the shear strain reaches to its maximum value in the Zn interlayer, the initial failure occur in the ZnMg layer and leads to a local drop of the shear strain in the Zn interlayer to compensate the strain raise. This process is repeated during the scratch test and causes periodic failure in the bi-layered coating sample. For the single layer ZnMg coating, the delamination is not periodic, and follows by removal of the coating material on the forward side (see Fig. 13c and d) and yet a long crack propagates along the interface on the backward side. Furthermore, the critical load in which the first failure occurs is obtained as 8 N and 12.5 N for the single layer and the bi-layer coatings, respectively. Therefore, the ductile zinc interlayer can effectively detain the onset of failure in the ZnMg coating. The same behavior is also observed even for different ZnMg alloys having various mechanical properties and it emphasizes that the presence of the Zn interlayer is essential for the enhancement of the adhesion between steel substrate and the ZnMg coatings.

As discussed before, ZnMg single layer coatings always show inferior adhesion to the steel compared to the bi-layer ZnMg-Zn. As an

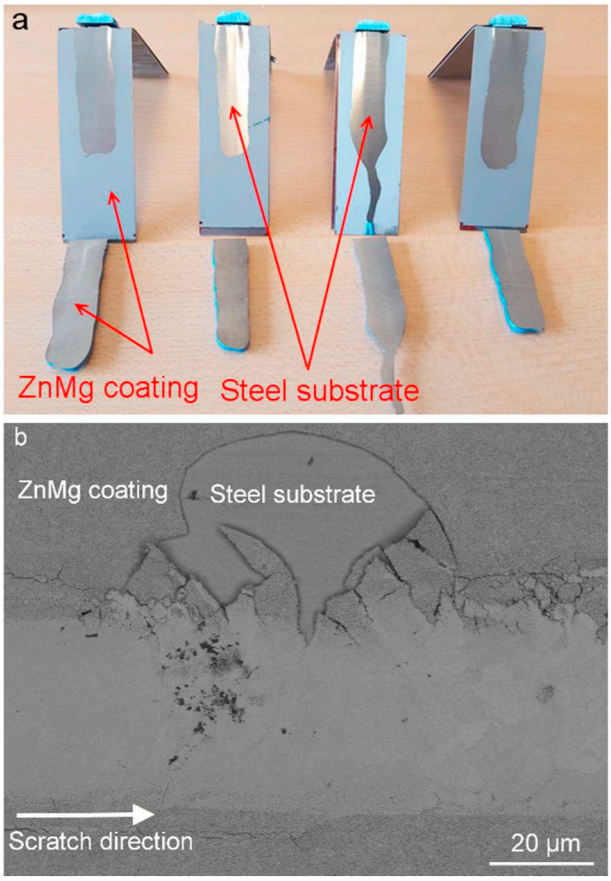

Fig. 14. (a) BMW crash adhesion test for ZnMg4.5 single layer coating indicating poor adhesion of the coating to the substrate; (b) Brittle failure of the ZnMg4.5 single layer coating during scratch test at $L_C \cong 7$ N.

example, Fig. 14a shows the BMW crash adhesion test results for the single layer ZnMg4.5 coating deposited on the DP800 steel substrate. As can be seen, the single layer ZnMg coating was tested four times, and totally detached from the steel substrate during bending and therefore do not pass the BMW adhesion tests. Scratch test shows the same failure behavior of the ZnMg single layer coating as the brittle delamination was also observed, see Fig. 14b. A large chip of the coating peels off from the scratch far to the side.

4. Conclusions

The effect of the Mg concentration on the microstructure, mechanical properties and the adhesion strength of ZnMg coatings were investigated. The main conclusions are summarized as follows:

- The hardness and the elastic modulus of ZnMg PVD coatings increase with the increase of Mg content up to 7.4 wt% and remains constant at higher Mg concentrations.
- Finite element analysis showed that ZnMg single layer coating always fails at lower critical loads than ZnMg-Zn bi-layer coatings during scratch test.
- The insertion of a zinc interlayer between ZnMg and steels substrate is essential for the adequate adhesion of ZnMg coatings in practical applications.
- It is found that the critical load of scratch test, L_C, is not a suitable criterion to compare the adhesion performance of ZnMg-Zn bi-layer coatings with different thickness and/or mechanical properties combinations. Instead, the Benjamin-Weaver model has been modified to quantify the adhesion strength of PVD ZnMg-Zn bi-layered coatings with scratch test, which reveals consistent results with the BMW crash adhesion test.
- The optimum range of Mg content for the ZnMg top layer was determined as 5.8–7.4 wt%. The adhesion strength drops at higher Mg contents.

Acknowledgment

This research was carried out under project number S22.3.13513a in the framework of the Partnership Program of the Materials innovation institute M2i (www.m2i.nl) and the Technology Foundation TTW (www.stw.nl), which is part of the Netherlands Organization for Scientific Research (www.nwo.nl).

References

[1] A.R. Marder, The metallurgy of zinc-coated steel, Prog. Mater. Sci. 45 (2000) 191–271.
[2] S.M.A. Shibli, B.N. Meena, R. Remya, A review on recent approaches in the field of hot dip zinc galvanizing process, Surf. Coat. Technol. 262 (2015) 210–215.
[3] G.M. Song, T. Vystavěl, N. Van der Pers, J.Th.M. De Hosson, W.G. Sloof, Relation between microstructure and adhesion of hot dip galvanized zinc coatings on dual phase steel, Acta Mater. 60 (2012) 2973–2981.
[4] R.P. Edavan, R. Kopinski, Corrosion resistance of painted zinc alloy coated steels, Corros. Sci. 51 (2009) 2429–2442.
[5] Y. Li, Corrosion behaviour of hot dip zinc and zinc-aluminium coatings on steel in seawater, B. Mater. Sci 24 (2001) 355–360.
[6] S.W. Li, B. Gao, S.H. Yin, G.F. Tu, G.L. Zhu, S.C. Sun, X.P. Zhu, The effects of RE and Si on the microstructure and corrosion resistance of Zn–6Al–3Mg hot dip coating, Appl. Surf. Sci. 357 (2015) 2004–2012.
[7] J. Kawafuku, J. Katoh, M. Toyama, K. Ikeda, H. Nishimoto, H. Satoh, Properties of zinc alloy coated steel sheets obtained by continuous vapor deposition pilot-line, Proceedings of 5th Automotive Corrosion & Prevention Conference, Michigan, USA, (1991).
[8] M.M. Koyama, M. Murase, Y. Mori, Improvement in the corrosion resistance of zinc-plated steels by electrodeposition of magnesium from a molten salt, ISIJ Int. 36 (1996) 714–719.
[9] M.M.K. Koyama, Y. Mori, Inhibition of anodic dissolution of zinc-plated steel by electrodeposition of magnesium form a molten salt, ISIJ Int. 37 (1997) 55–58.
[10] M. Morishita, K. Koyama, Y. Mori, Self-healing ability of zinc-plated steel coated with magnesium electrodeposited form a molten salt, Mater. Trans. JIM 38 (1997) 719–723.
[11] B. Schuhmacher, C. Schwerdt, U. Seyfert, O. Zimmer, Innovative steel strip coatings by means of PVD in a continuous pilot line: process technology and coating development, Surf. Coat. Technol. 163 (2003) 703–709.
[12] N.C. Hosking, M.A. Strom, P.H. Shipway, C.D. Rudd, Corrosion resistance of zinc-magnesium coated steel, Corros. Sci. 49 (2007) 3669–3695.
[13] J. Winiarski, W. Tylus, B. Szczygie, EIS and XPS investigations on the corrosion mechanism of ternary Zn–Co–Mo alloy coatings in NaCl solution, Appl. Surf. Sci. 364 (2016) 455–466.
[14] M.S. Kim, J.H. Kwak, J.S. Kim, Y.H. Liu, N. Gao, N.Y. Tang, Galvanizability of advanced high-strength steels 1180TRIP & 1180CP, Metall. Mater. Trans. A 40A (2009) 1903–1910.
[15] M.J. Carr, M.J. Robinson, The effects of zinc alloy electroplating on the hydrogen embrittlement of high strength steels, Trans. Inst. Met. Finish. 73 (1995) 58–64.
[16] B. Navinsek, P. Panjan, I. Milosev, PVD coatings as an environmentally clean alternative to electroplating and electroless processes, Surf. Coat. Technol. 116-119 (1999) 476–487.
[17] W.S. Jung, C.W. Lee, T.Y. Kim, B.C. De Cooman, Mg content dependence of EML-PVD Zn-Mg coating adhesion on steel strip, Metall. Mater. Trans. A 47 (2016) 4594–4605.
[18] J.H. La, K.T. Bae, S.Y. Lee, K.H. Nam, A hybrid test method to evaluate the adhesion characteristics of soft coatings on steel substrates - application to Zn-Mg coated steel, Surf. Coat. Technol. 307 (2016) 1100–1106.
[19] M. Lee, I. Bae, Y. Kwak, K. Moon, Effect of interlayer insertion on adhesion properties of ZnMg thin films on steel substrate by PVD method, Curr. Appl. Phys. 12 (2012) S2–S6.
[20] E. Zoestbergen, J. van de Langkruis, T.F.J. Maalman, E. Batyrev, Influence of diffusion on the coating adhesion of zinc-magnesium thin films onto steel, Surf. Coat. Technol. 309 (2017) 904–910.
[21] J. La, M.G. Song, H.K. Kim, S.Y. Lee, W.S. Jung, Effect of deposition temperature on microstructure, corrosion behavior and adhesion strength of ZnMg coatings on mild steel, J. Alloys Compd. 739 (2018) 1097–1103.
[22] A.R. Miedema, R. Boom, F.R. de Boer, On the heat of formation of solid alloys, J. Less-Common Met. 41 (1975) 283–298.
[23] G.J. Vander Kolk, A.R. Miedema, A.K. Niessen, On the composition range of amorphous binary transition metal alloys, J. Less-Common Met. 145 (1988) 1–17.
[24] T. Egami, Y. Waseda, Atomic size effect on the formability of metallic glasses, J. Non-Cryst. Solids 64 (1984) 113–134.
[25] A.R. Miedema, P.F. de Chatel, F.R. de Boer, Cohesion in alloys- fundamentals of a semi-empirical model, Physica B 100 (1980) 1–28.

[26] P.I. Loeff, A.W. Weeber, A.R. Miedema, Diagrams of formation enthalpies of amorphous alloys in comparison with crystalline solid solution, J. Less-Common Met. 140 (1988) 299–305.
[27] E.A. Brands, Smithells Metals Reference Book, 6th ed., Butterworths, London, 1983.
[28] C.C. Kammerer, S. Behdad, L. Zhou, F. Betancor, M. Gonzalez, B. Boesl, Y.H. Sohn, Diffusion kinetics, mechanical properties, and crystallographic characterization of intermetallic compounds in the Mg-Zn binary system, Intermetallics 67 (2015) 145–155.
[29] A. Leyland, A. Matthews, On the significance of the H/E ratio in wear control: a nanocomposite coating approach to optimised tribological behavior, Wear 246 (2000) 1–11.
[30] A.A.C. Recco, I.C. Oliveira, M. Massi, H.S. Maciel, A.P. Tschiptschin, Adhesion of reactive magnetron sputtered TiN_x and TiC_y coatings to AISI H13 tool steel, Surf. Coat. Technol. 202 (2007) 1078–1083.
[31] D. Craciun, N. Stefan, G. Socol, G. Dorcioman, E. McCumiskey, M. Hanna, C.R. Taylor, G. Bourne, E. Lambers, K. Siebein, V. Craciun, Very hard TiN thin films grown by pulsed laser deposition, Appl. Surf. Sci. 260 (2012) 2–6.
[32] M. Dao, N. Chollacoop, K.J. Van Villet, T.A. Venkatesh, S. Suresh, Computational modeling of the forward and reverse problems in instrumented sharp indentation, Acta Mater. 49 (2009) 3899–3918.
[33] P.A. Stieinmann, Y. Tardy, H.E. Hintermann, Adhesion testing by the scratch test method, the influence of intrinsic and extrinsic parameters on the critical load, Thin Solid Films 154 (1987) 333–349.
[34] J. Valli, A review of adhesion test methods for thin hard coatings, J. Vac. Sci. Technol. 4 (1986) 3007–3014.
[35] P. Benjamin, C. Weaver, Measurements of adhesion of thin films, Proc. R. Soc. Lond. 254 (1960) 163–176.
[36] C. Weaver, Adhesion of thin films, J. Vac. Sci. Technol. 12 (1975) 18–25.
[37] S.J. Bull, E.G. Berasetegui, An overview of the potential of quantitative coating adhesion measurement by scratch testing, Tribol. Int. 39 (2006) 99–114.
[38] G.M. Song, W.G. Sloof, Y.T. Pei, J.Th M. De Hosson, Interface fracture behavior of zinc coatings on steel: experiments and finite element calculations, Surf. Coat. Technol. 201 (2006) 4311–4316.
[39] G.M. Song, J.T.M. De Hosson, W.G. Sloof, Y.T. Pei, Evaluation of interface adhesion of hot dipped zinc coating on TRIP steel with tensile testing and finite element calculation, WIT Trans. Eng. Sci. 91 (2015) 3–14.
[40] T. Prosek, A. Nazarov, U. Bexell, D. Thierry, J. Serak, Corrosion mechanism of model zinc-magnesium alloys in atmospheric conditions, Corros. Sci. 50 (2008) 2216–2231.